Journal of
Materials Chemistry C

Materials for optical and electronic devices
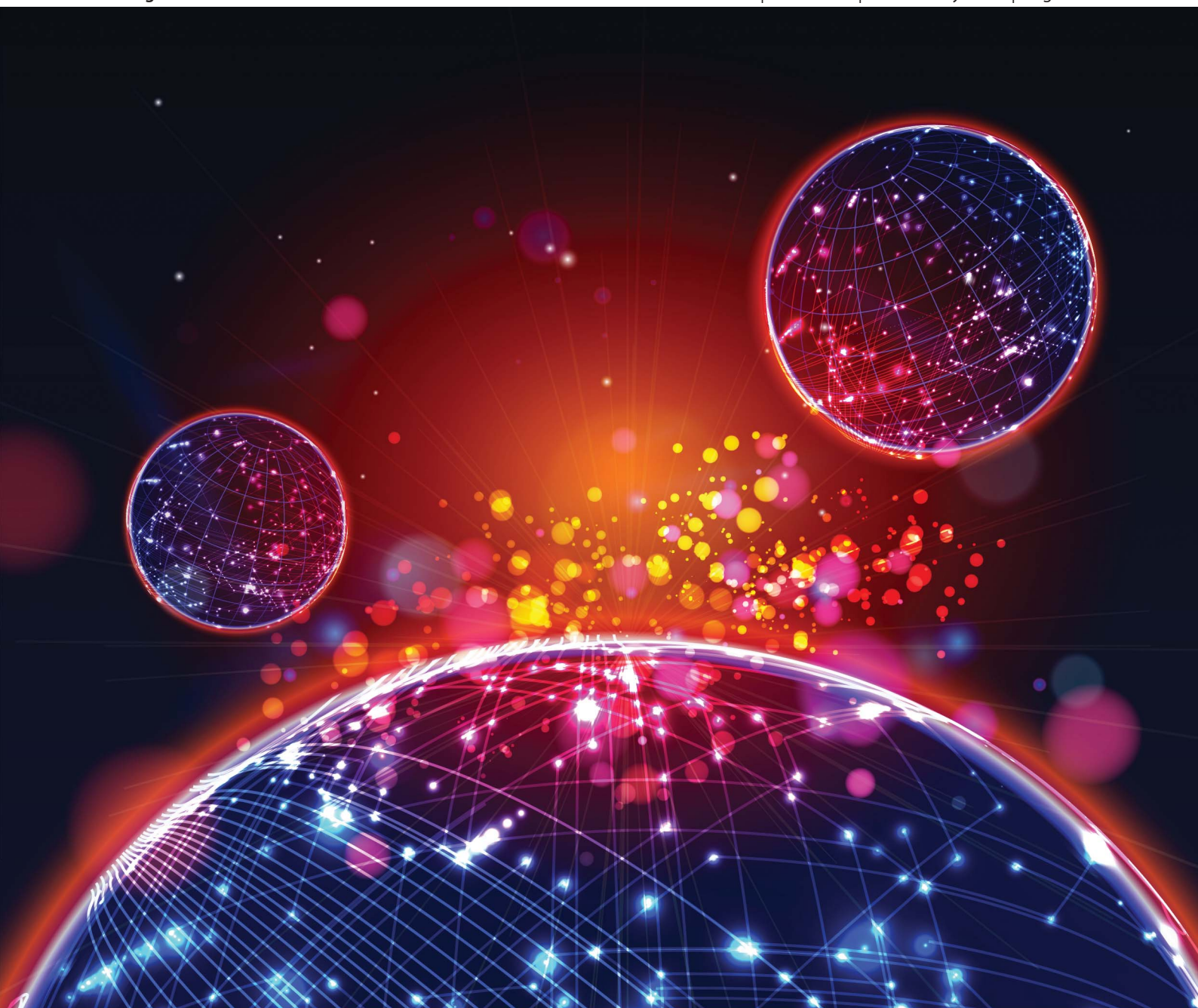
PAPER
Jin Jang *et al.*
Inverted quantum-dot light-emitting diodes with solution-processed
aluminium–zinc oxide as a cathode buffer

PAPER

Inverted quantum-dot light-emitting diodes with solution-processed aluminium–zinc oxide as a cathode buffer†

Hyo-Min Kim, Jun-Ho Youn, Gi-Jun Seo and Jin Jang*

We report an inverted structure of quantum-dot light emitting diodes (QLEDs) with a metal oxide as a cathode buffer. The Al doped zinc oxide (AZO) with Al concentration from 0 to 30% was used as a charge transport layer in QLEDs which were processed at the temperature of 225 °C. It is found that the conductivity of AZO decreases with increasing Al concentration, but the luminance intensity increases from 6380 to 26 700 cd m^{-2}. The current and power efficiencies at 1000 cd m^{-2} increase from 3.03 to 4.63 cd A^{-1} and 2.75 to 3.64 lm W^{-1}, respectively, as the Al concentration increases from 0 to 30%. The luminance intensity for the QLED with 30% AZO increases further to 31 030 cd m^{-2} and the current efficiency to 5.21 cd A^{-1} by increasing the thickness of the electron transport layer from 33 to 50 nm. It is concluded therefore that a solution processed AZO can be an effective cathode buffer for an inverted structure of QLEDs.

Introduction

Quantum-dot light emitting diodes (QLEDs) are of increasing interest as an emerging light source, since they have the advantages of good color purity and ease of color tunability.[1,2] It is noted that quantum dots have high photoluminescence efficiency at room temperature because of strong binding of electrons in a quantum dot.[3] The color in QLEDs can be easily tuned by varying the core size of quantum dots (QDs) without changing the device structure and materials.[4]

One of the important factors in achieving high efficiency LEDs and QLEDs is related to the optimization of the structures for achieving improved light extraction in LEDs and QLEDs. Especially, recent works using defective grating micro-lens arrays in LEDs[5] based on the self-assembly rapid convective deposition process[6,7] have been shown to improve the power conversion efficiency of the devices by 3 times.

The current work on QLEDs is focused on the investigation of primary application for display technologies. Significant advances have also been achieved in improving the internal quantum efficiency (IQE)[8–11] and extraction efficiency in inorganic LEDs.[12–14] These results can contribute to achieve high efficiency QLEDs for light application.

By using QDs with different core sizes, the devices can have light emissions over a broad wavelength range.[15] The color of the QD depends on its core size even though the highest

occupied molecular orbital (HOMO) and the lowest unoccupied molecular orbital (LUMO) levels of QDs are the same. Therefore, it is possible to tune the color by using different QD sizes with the same light emitting diode structure. Since QDs are inorganic materials, they are more stable against moisture and oxygen exposures as compared to organic materials used for light emission.[16] However, QLEDs have issues such as material stability, QD particle aggregation and uniform layer formation because of their small size (3–7 nm). It is also noted that the under-layer of QD should have a smooth surface morphology to have a uniform QD coating.

It is known that metal oxides can be used as a charge transport layer in OLEDs and QLEDs.[2,16,17] Generally, amorphous metal oxides have poor conductivity when processed at low temperatures, also metal oxides in the amorphous phase have lower carrier mobility compared to their crystalline counterparts.[18] Note that the crystallization of metal oxides takes place generally at higher temperatures (>200 °C). Therefore, the use of metal oxides has many issues in the conventional QLED structure because a quite high temperature process is needed to achieve high conductivity. Note that the QD layer should not be damaged during the processing of the layers on top of it.[19] The maximum process temperature is determined by the organic ligands on QDs which can be easily damaged by annealing at a higher temperature. Therefore, the maximum process temperature of a metal oxide should not exceed that (~180 °C) of the QD curing temperature. Therefore, we propose an inverted structure in order to have an optimized process temperature which is independent of the QD annealing temperature.

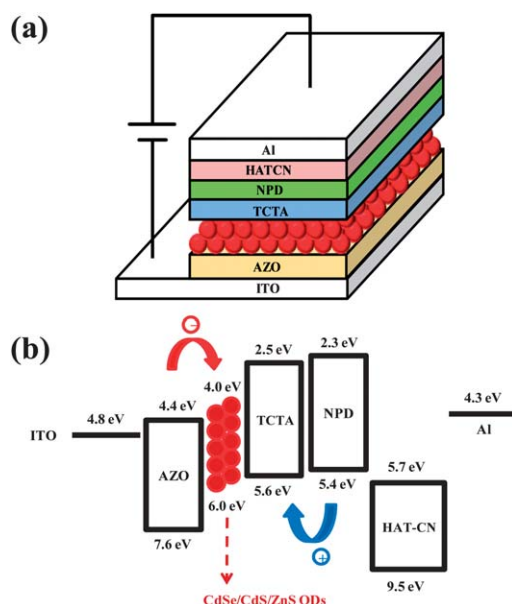The inverted structure is useful for active-matrix (AM) OLEDs and QLEDs with n-channel thin-film transistors (TFTs) such as

Department of Information Display and Advanced Display Research Center, Kyung Hee University, Seoul, Korea. E-mail: jjang@khu.ac.kr

† Electronic supplementary information (ESI) available. See DOI: 10.1039/c2tc00339b

This journal is © The Royal Society of Chemistry 2013

J. Mater. Chem. C, 2013, **1**, 1567–1573 | **1567**

oxide TFTs. Oxide TFTs can be used for large size AM displays because of large area deposition of the oxide semiconductor by sputtering and its higher mobility than that of amorphous silicon. They show mostly n-channel behavior and thus the inverted structure of QLED with a bottom cathode is preferred.[20] In the case of inverted top-emitting OLEDs, indium-tin-oxide (ITO) is widely used as the anode and deposited by sputtering on the top of the organic layer. In this case, radiation damage to the organic layer during ITO deposition can degrade the performances of OLEDs.[21] On the other hand, the inverted bottom-emitting OLEDs do not have such problems because the ITO anode is first deposited and then the QD layer is coated.[20,22]

Among metal oxides, zinc oxide (ZnO) and doped ZnO films have received much attention due to their excellent optical and electrical properties.[23] ZnO can be doped by adding elements such as boron (Br), aluminium (Al), indium (In), gallium (Ga) and so on.[24] Conductivity of the n-type Al doped ZnO (AZO) is affected by intrinsic defects, interstitial zinc and oxygen vacancies[25] and it can be used as a transparent conducting oxide and has been used as back-contact for copper indium gallium selenide (CIGS) solar cells.[26] Also, sol–gel coating of AZO has been used in organic photovoltaic (OPV) cells[27] since it is simple and can be a low-cost process over a large area. In this work, we applied sol–gel coated AZO as a cathode buffer in inverted QLEDs.

An inverted structure of QLEDs with a ZnO nanoparticle layer as the ETL has recently been demonstrated.[28] As shown in Fig. 5 Al incorporation in sol–gel processed ZnO is found to increase the performance of QLEDs. It is interesting that 30% Al in ZnO leads to the best results in this work.

Experimental

We used the AZO layers with various Al concentrations of 0, 2, 4, 6, 10, 15, 20 and 30%. In the case of preparing 2% sol–gel solution, zinc acetate dihydrate ($Zn(C_4H_6O_4) \cdot 2H_2O$) 2.20 g and 2.0% of aluminium hydroxide acetate ($HOAl(C_2H_3O_2)_2$)) were mixed together in a three necked beaker. Monoethanolamine (MEA) was mixed with AZO powders in order to have a stable AZO complex. The AZO complex was dissolved in 100 mL ethanol and then refluxed at 80 °C for 9 h at the stirring speed of 400 rpm until transparent solution was obtained. The coated thin-films were heated at 225 °C for 10 min in air.[29] Then, QDs of 626 nm CdSe/CdS/ZnS (core/shell/shell type) (QD Solution, Korea) were used for QLEDs, having LUMO and HOMO levels of 4.0 and 6.0 eV, respectively.[30]

In this experiment, the ZnO or AZO layer is used as the electron transport layer. The thickness of the ETL was fixed at 30–33 nm. Fig. 1(a) shows the structure of the inverted QLED: ITO/AZO (30–33 nm)/CdSe/CdS/ZnS QDs (10–15 nm)/4,4′,4′′-tri(N-carbazolyl)triphenylamine (TCTA) (10 nm)/N,N′-bis(naph-thalene-1-yl)-N,N′-bis(phenyl)-2,2′-dimethylbenzidine (α-NPD) (20 nm)/dipyrazino[2,3-f:2′,3′-h]quinozaline-2,3,6,7,10,11-hexa-carbonitrile (HAT-CN) (20 nm)/Al (100 nm) and Fig. 1(b) shows
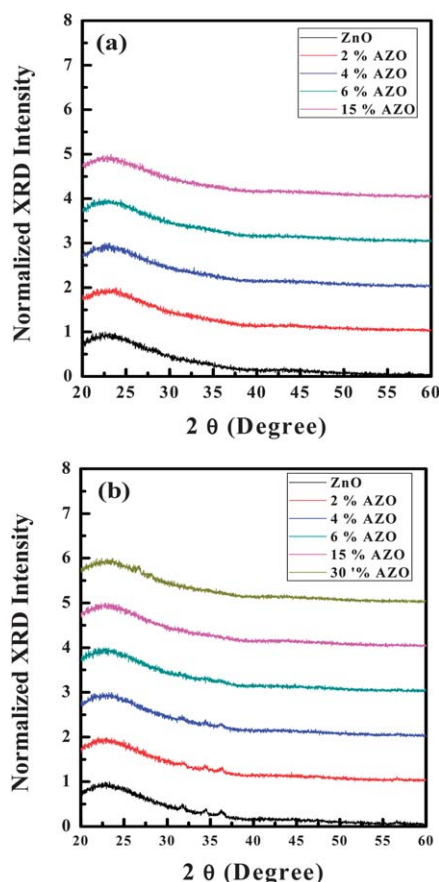

Fig. 1 (a) Schematic cross-sectional view and (b) energy band diagram of inverted QLEDs with solution processed AZO. Electrons and holes are generated at the NPD/HATCN interface[38] and holes transport to the QD side and the electrons to the anode.

Fig. 2 XRD data of AZO films with various Al concentrations in ZnO annealed at (a) 225 °C and (b) 500 °C. All samples were annealed in air. The crystalline peaks (31.77°, 34.47° and 36.29°) can be seen for the un-doped and less than 4% doped ZnO films.

1568 | J. Mater. Chem. C, 2013, **1**, 1567–1573

This journal is © The Royal Society of Chemistry 2013

the energy band diagram of an inverted QLED with AZO, which was fabricated using the following procedure. An AZO layer was spin-coated at 500 rpm onto a UV plasma-treated ITO having a sheet resistance of 10–15 Ω sq^{-1} and then annealed at 225 °C for 10 min in ambient air. After baking the AZO layer, CdSe/CdS/ZnS QDs, with an average diameter of 7–8 nm, in toluene (concentration 5.0 mg mL^{-1}) were spin-coated at 2500 rpm and then heated at 190 °C for 10 min in a N_2 filled glove box. Our QDs had 1.9 eV of optical band-gap for the film made by drop-casting and a photoluminance (PL) peak at 628 nm with a Full-Width at Half-Maximum (FWHM) of 33 nm as shown in Fig. S1 (ESI†). The TCTA layer acts as the hole transport and electron blocking layer (HTL and EBL), α-NPD as a HTL and HAT-CN as a hole injection layer (HIL) were deposited by thermal evaporation. Then, an Al (100 nm) layer was deposited on the top as an anode by thermal evaporation. Finally, the devices were encapsulated with glass in a glove box with a N_2 environment.

The current density–voltage (J–V), luminance–voltage (L–V), EL spectrum and EQE characteristics were measured using a Konica Minolta CS100A luminance meter and a CS1000A spectrometer coupled with a Keithley 2635A voltage and current source meter.

Results and discussion

Fig. 2 shows the X-Ray Diffraction (XRD) spectra of AZO films with various Al concentrations in ZnO. The samples were annealed at 225 °C in air and the thickness was ~33 nm. Fig. 2(a) shows that the crystalline peaks could not be found in the XRD spectra of the AZO films annealed at 225 °C, indicating that the AZO films are amorphous. In the other studies, solution processed AZO films are generally crystallized at 500–700 °C in air[31] and crystalline AZO films exhibit a peak at 34–35° (ref. 31 and 32) in the XRD spectra. Thus, we annealed the samples at 500 °C in air, and we could find a crystalline peak in the films as shown in Fig. 2(b). The crystalline peaks in ZnO and AZO films were found to be between 31° and 37°, but only in ZnO and AZO layers with less than 4% Al doping. Therefore, it is concluded that the AZO films are amorphous and that the amorphous phase is more dominant as the Al concentration increases in ZnO.

Fig. 3 shows the Atomic Force Microscopy (AFM) data of the AZO films with various Al concentrations: (a), (b), (c) and (d) are ZnO, 2% AZO, 6% AZO and 15% AZO, respectively. The Root Mean Square (RMS) roughness of ZnO and 2% AZO was 2.02 nm and 0.34 nm, respectively. The surface roughness data are summarized in Table 1, such as peak to valley (R_{pv}), roughness root mean square (R_q) and average roughness (R_a). It is noted that the roughness can be decreased by Al doping in a sol–gel processed ZnO film. Because the AZO layer is underneath the QD layer, the roughness of AZO affects the QDs layer formation and thus the electrical properties of QLEDs.

The insertion of the Al content in ZnO leads to a decrease of its RMS roughness. Al doping can modify the surface to have less surface roughness until 2% Al doping. On the other hand, when the Al concentration is higher than 2% the material changes to alloy, which can increase the surface roughness. Al content higher than 2% causes the film to be c-axis oriented,
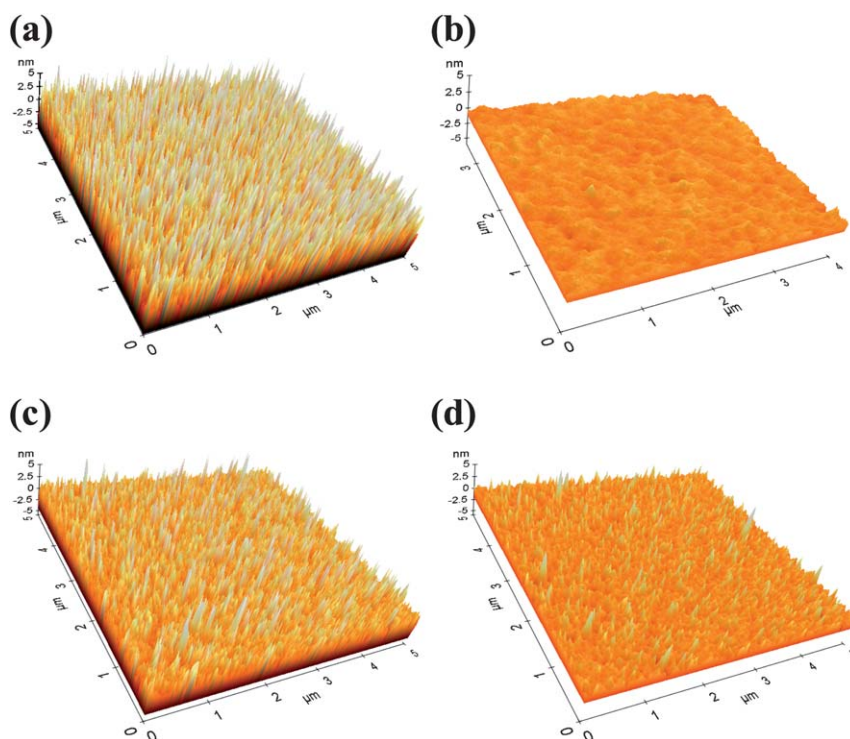
Fig. 3 AFM images of the AZO surfaces with various Al concentrations in ZnO: (a) ZnO, (b) 2% AZO, (c) 6% AZO, and (d) 15% AZO (all samples were annealed at 225 °C). The AZO films have smoother surface than that of the ZnO layer.

This journal is © The Royal Society of Chemistry 2013

J. Mater. Chem. C, 2013, **1**, 1567–1573 | **1569**

Table 1 AFM surface roughness data for ~33 nm Al doped ZnO films. Peak to valley (R_{pv}), roughness root mean square (R_q) and average roughness (R_a) are shown below

	Al doping % in ZnO (%)				
	0 (ZnO)	2	4	6	15
R_{pv} (nm)	14.81	2.82	3.72	11.79	7.05
R_q (nm)	2.02	0.34	0.35	1.17	0.57
R_a (nm)	1.62	0.27	0.28	0.88	0.42
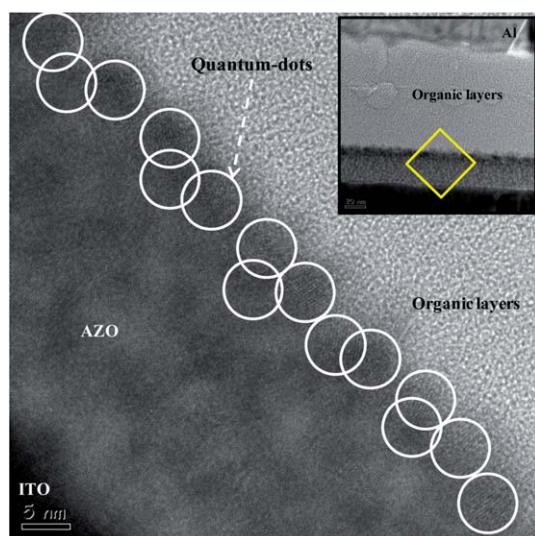
Fig. 4 TEM image of an inverted QLED with 4% AZO and the inset shows the TEM image of the device. The quantum dot layer can be seen with an average thickness of ~1.5 layer.

deteriorating the crystallinity of the film at the surface.[33] The amount of Al had a stronger c-axis orientation perpendicular to the substrate. Therefore, AZO surface roughness is increased with increasing Al concentration.

Fig. 4 shows the Transmission Electron Microscopy (TEM) image of the enlarged QDs layer in the device and the inset shows the cross-section of the QLED, where organic layers can be distinguished. The AZO thickness is 30–33 nm on ITO and there are 1–2 QD layers on AZO. With increasing QDs layer thickness, the current density and luminescence intensity decrease because of the poor carrier transport in QDs.[34]

Table 2 shows the conductivity values with various Al concentrations in the ZnO films. The entire samples were annealed at 225 °C in air and their thicknesses were ~33 nm. The ZnO film has a resistance of 50.21 MΩ, and the resistance of AZO increases with increasing Al concentration. Therefore, the

Table 2 Conductivity data for ~33 nm thick Al doped ZnO films annealed at 225 °C for 10 minutes
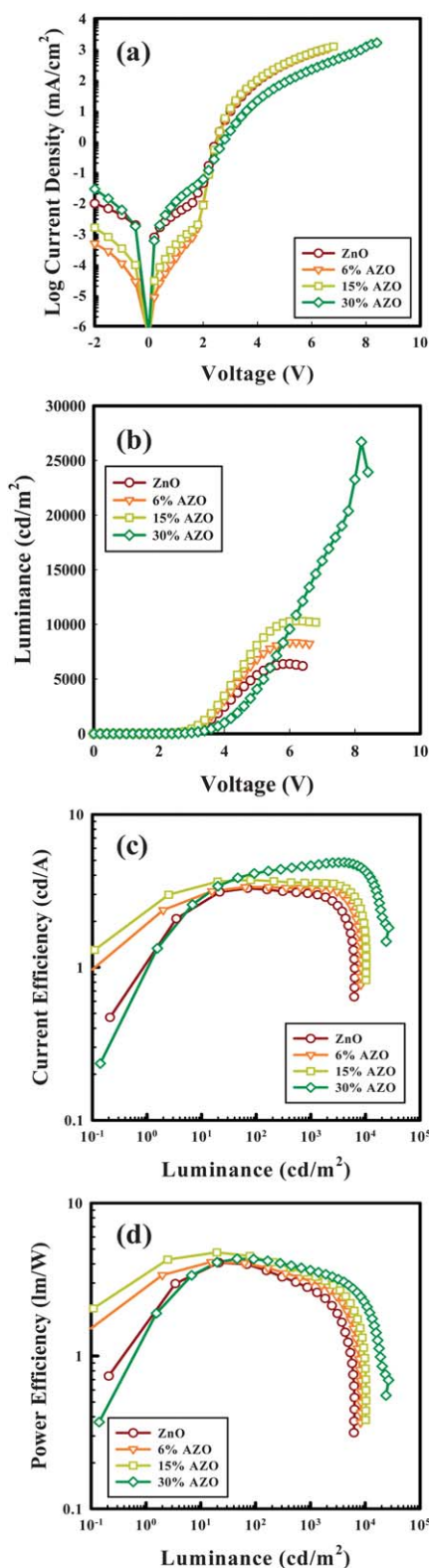
Al concentration in ZnO (%)	0 (ZnO)	6	20	30
σ (S cm^{-1})	2.44×10^{-4}	5.49×10^{-6}	1.22×10^{-8}	3.10×10^{-10}

conductivities of AZO films decrease with increasing Al concentration.

Fig. 5 shows the device characteristics of the QLEDs with various Al concentrations in AZO films with the same layer thickness. In this experiment, we used the layers of NPD of 20 nm and HAT-CN of 20 nm because device performance is the best in these conditions as shown in Fig. S2 and Table S1.† The maximum luminance is found to be 6380, 8348, 10 320 and 26 700 cd m^{-2} when the Al concentration is 0, 6, 15 and 30%, respectively. Note that the QD thickness is 7 to 15 nm (average 1.5 atomic layer) when the spin speed for QD coating is 2500 rpm. The inverted QLED shows the color coordinate of (0.69, 0.31), which indicates a deep-red similar to the phosphorescent deep-red of OLED (CIE$_x$ = 0.69 and CIE$_y$ = 0.31) made by Universal Display Corporation (UDC).[35] These devices have the turn-on voltages (V_T) of 1.90, 2.00, 1.98 and 1.94 V when the Al concentrations in AZO are 0, 6, 15 and 30%, respectively, and the driving voltages (V_D) are 2.67 V (ZnO), 2.67 V (6% AZO), 2.63 V (15% AZO) and 3.02 V (30% AZO). The holes and electrons are injected from an Al anode and an ITO cathode, respectively. Electrons are transported through AZO to the QDs and the AZO acts as a hole blocking layer (HBL) because of its deep HOMO level. Note that the HOMO levels of AZO and quantum dots are 7.6 and 6.0 eV, respectively. The TCTA layer acts as an electron blocking layer (EBL), owing to its lower LUMO level. The LUMO levels of quantum dots and TCTA are 3.9 and 2.5 eV, respectively, resulting in an accumulation of the electrons in the QDs and the TCTA layer. And the electrons can fill into the excited states of QDs. In the same manner, holes are accumulated in the AZO and the QDs. The main process of QD EL in QLEDs is as follows. When the bias was applied on the device, electrons and holes were injected from the cathode and anode into the ETL and the HTL, respectively. Electrons and holes were accumulated in QDs. The electrons trapped in excited states transit to the ground state, leading to the radiative e–h recombination. The quantum confinement of electrons at the QDs determines the color of the emitted light by the transition of electrons from the excited state to the ground state.[36] As shown in Fig. S3,† we could observe the only QD peak in the EL spectrum of our device due to confinement of carriers with high barriers of AZO and TCTA. These high barriers come from the higher HOMO level of AZO and the lower LUMO level of TCTA than those of QDs.

Resistivity of the QD layer is high so that optimization of its thickness is important for effective electron and hole injections to the QD layer for high quantum efficiency. In this work 1.5 multi-layers of QDs were found to be the optimum thickness. But it would be a single layer if QDs are regularly distributed without any vacancy. If the QDs do not completely cover the interface between AZO and TCTA, accumulated electrons and holes can pass through the QD layer without contributing to light emission. Therefore, more than one mono-layer of QDs should be fully covered on the under-layer to achieve high efficiency.

Fig. 6 shows the summarized device characteristics with various Al concentrations in AZO films. Luminance intensity increases as the Al concentration in ZnO increases as shown in Fig. 6(a) from 0 to 30%. Note that also Al doping in ZnO

1570 | J. Mater. Chem. C, 2013, **1**, 1567–1573

This journal is © The Royal Society of Chemistry 2013

Fig. 5 (a) Current density–voltage, (b) luminance–voltage, (c) current efficiency–luminance and (d) power efficiency–luminance for the devices with fixed NPD/HAT-CN thickness (20 nm/20 nm) and various Al concentrations in ZnO (ZnO: dark red circle, 6% AZO: orange triangle down, 15% AZO: green square and 30% AZO: dark green diamond).
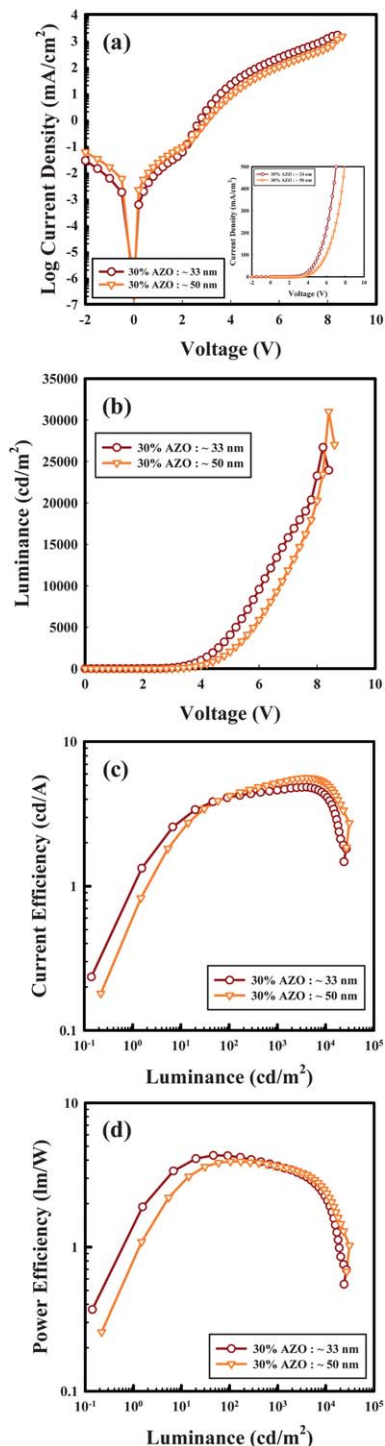
increases the band-gap.[37] The increase of the band-gap of AZO with Al concentration leads to an increase of the hole energy barrier between HOMO levels of QDs and that of AZO and thus the holes accumulated at the QD layer could not cross the AZO to the cathode. Therefore, the probability of recombination between the hole and the electron can increase in QD layers. As a result, the luminance intensity increases with increasing Al concentration. Fig. 6(c) shows the relationship between current and power efficiencies *versus* Al concentrations. Note that the efficiency increases slightly with increasing Al concentration in ZnO.

The brightness increases with increasing Al concentration in ZnO up to 30%. Note that the surface is smooth and has an amorphous phase with increasing Al concentration in AZO as shown in Fig. 2 and 3. The AZO annealed at 225 °C has an amorphous phase and is expected to have higher conductivity than AZO processed at 180 °C.

Fig. 7 shows the device characteristics with different ETL thickness of 30% AZO. We compared ETL thicknesses between ~33 nm and ~50 nm. ETL thickness affects the device characteristics as shown in Fig. S4 and Table S2.† The device characteristics can be improved by increasing the ETL thickness to ~50 nm. The luminance intensity and maximum current efficiency increase from 26 700 to 31 030 cd m^{-2} and from
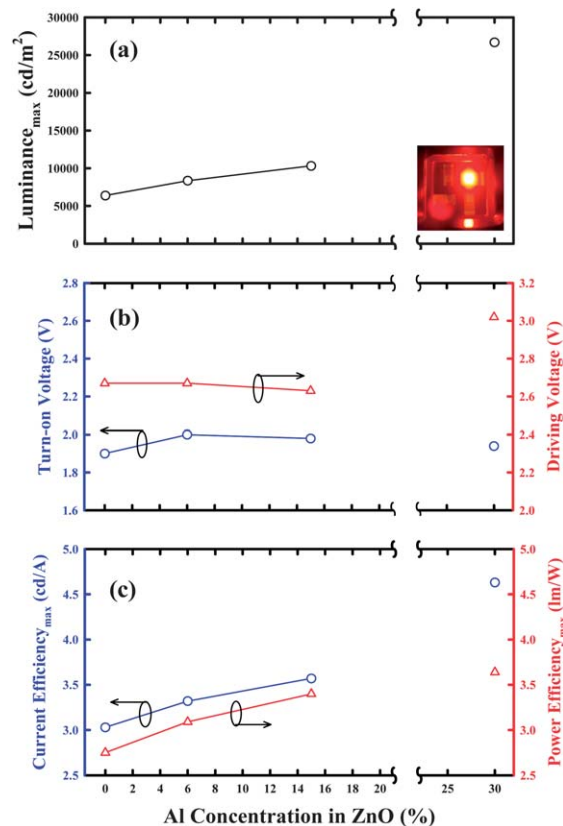
Fig. 6 Summarized device characteristics with various Al concentrations in AZO films. (a) Maximum luminance—Al concentrations in ZnO, (b) V_T and V_D—Al concentrations in ZnO, (c) current and power efficiencies—Al concentrations in ZnO at 1000 cd m^{-2}. The inset in (a) indicates the light emission from QLEDs.

This journal is © The Royal Society of Chemistry 2013

J. Mater. Chem. C, 2013, **1**, 1567–1573 | **1571**

Fig. 7 (a) Log current density–voltage (inset: current density–voltage in linear scale), (b) luminance–voltage, (c) current efficiency–luminance and (d) power efficiency–luminance characteristics for the devices with different ETL (30% AZO) thickness using a fixed NPD/HAT-CN thickness (20 nm/20 nm).

4.86 to 5.65 cd A^{-1}, respectively. Also, the current efficiency at 1000 cd m^{-2} increases from 4.63 to 5.21 cd A^{-1}. But, the power efficiency at 1000 cd m^{-2} decreases. In the inset graph of Fig. 7(a), the current density plot of OLEDs with 50 nm AZO shifts to positive voltage as compared to that with 33 nm AZO because the current density is related to resistivity, and the

resistivity is related to the thickness of the layers. However, even though the current density shifts to positive voltage, the device characteristics are improved by the charge balance between electrons and holes in the EML.

The electron mobility and layer thickness are important for matching the charge balance between electrons and holes and thus for performance improvement. The conductivity decreases with increasing Al concentration in AZO, resulting in the decrease of currents in the metal oxide ETL.[37] Because hole transport layers are fixed in our device, the charge balance can be adjusted by varying the ETL (AZO) thickness. This improvement is due to the well-matched charge balance in the EML with highly resistive AZO.

Conclusions

We demonstrated the inverted structure of the QLEDs exhibiting a deep-red color (0.69, 0.31) using a solution processed AZO layer on ITO. The devices exhibited an increase in the maximum luminance with increasing Al concentration because of the smooth surface and less electrical conductivity of AZO. When the Al concentration in ZnO increases from 0 to 30%, the luminance intensity, current efficiency and power efficiency at 1000 cd m^{-2} increase from 6380 to 26 700 cd m^{-2}, from 3.03 to 4.63 cd A^{-1} and from 2.75 to 3.64 lm W^{-1}, respectively. The luminance intensity increases from 26 700 to 31 030 cd m^{-2} by increasing the AZO thickness from 33 to 50 nm. Therefore, the solution processed AZO film can be used as an effective cathode buffer for QLEDs.

Acknowledgements

Notes and references

1 K. S. Cho, E. K. Lee, W. J. Joo, E. J. Jang, T. H. Kim, S. J. Lee, S. J. Kwon, J. Y. Han, B. K. Kim, B. L. Choi and J. M. Kim, *Nat. Photonics*, 2009, **3**, 341.

2 V. Wood, M. J. Panzer, J. E. Halpert, J. M. Caruge, M. G. Bawendi and V. Bulovic, *ACS Nano*, 2009, **3**, 3581.

3 B. H. Kang, J. S. Seo, S. H. Jeong, J. H. Lee, C. S. Han, D. E. Kim, K. J. Kim, S. H. Yeon, D. H. Kwon, H. R. Kim and S. W. Kang, *Opt. Express*, 2010, **18**, 18303.

4 Q. Sun, Y. A. Wang, L. S. Li, D. Wang, T. Zhu, J. Xu, C. Yang and Y. Li, *Nat. Photonics*, 2007, **1**, 717.

5 W. H. Koo, W. Youn, P. Zhu, X. H. Li, N. Tansu and F. So, *Adv. Funct. Mater.*, 2012, **22**, 3454.

6 Y. K. Ee, R. A. Arif, N. Tansu, P. Kumnorkaew and J. G. Gilchrist, *Appl. Phys. Lett.*, 2007, **91**, 221107.

7 P. Kumnorkaew, Y. K. Ee, N. Tansu and J. F. Gilchrist, *Langmuir*, 2008, **24**, 12150.

8 R. M. Farrell, E. C. Young, F. Wu, S. P. Denbaars and J. S. Speck, *Semicond. Sci. Technol.*, 2012, **27**, 024001.

1572 | *J. Mater. Chem. C*, 2013, **1**, 1567–1573

This journal is © The Royal Society of Chemistry 2013

9 H. Zhao, G. Liu, J. Zhang, J. D. Poplawsky, V. Dierolf and N. Tansu, *Opt. Express*, 2011, **19**(S4), A991.

10 Y. K. Ee, J. M. Biser, W. Cao, H. M. Chan, R. P. Vinci and N. Tansu, *IEEE J. Sel. Top. Quantum Electron.*, 2009, **15**, 1066–1072.

11 H. Zhao, J. Zhang, G. Liu and N. Tansu, *Appl. Phys. Lett.*, 2011, **98**, 151115.

12 X. H. Li, R. Song, Y. K. Ee, P. Kumnorkaew, J. F. Gilchrist and N. Tansu, *IEEE Photonics J.*, 2011, **3**, 489.

13 E. Rangel, E. Matioli, Y. S. Choi, C. Weisbuch, J. S. Speck and E. L. Hu, *Appl. Phys. Lett.*, 2011, **98**, 081104.

14 J. J. Wierer, A. David and M. M. Megens, *Nat. Photonics*, 2009, **3**, 163.

15 J. Zhao, J. Zhang, C. Jiang, J. Bohnenberger, T. Basche and A. Mews, *J. Appl. Phys.*, 2004, **96**, 3206.

16 J. W. Stouwdam and R. A. J. Janssen, *J. Mater. Chem.*, 2008, **18**, 1889.

17 B. S. Mashford, T. L. Nguyen, G. J. Wilson and P. Mulvaney, *J. Mater. Chem.*, 2010, **20**, 167.

18 X. Feng, K. Shankar, O. K. Varghese, M. Paulose, T. J. Latempa and C. A. Grimes, *Nano Lett.*, 2008, **8**, 3781.

19 J. M. Caruge, J. E. Halpert, V. Wood, V. Bulovic and M. G. Bawendi, *Nat. Photonics*, 2008, **2**, 247.

20 S. Y. Chen, T. Y. Chu, J. F. Chen, C. Y. Su and C. H. Chen, *Appl. Phys. Lett.*, 2006, **89**, 053518.

21 J. Meyer, T. Winkler, S. Hamwi, S. Schmale, H. H. Johannes, T. Weimann, P. Hinze, W. Kowlasky and T. Riedl, *Adv. Mater.*, 2008, **20**, 3839.

22 M. Pfeiffe, S. R. Forrest, X. Zhou and K. Leo, *Org. Electron.*, 2003, **4**, 21.

23 H. Kind, H. Q. Yan, B. Messer, M. Law and P. D. Yang, *Adv. Mater.*, 2002, **14**, 158.

24 H. Sato, T. Minami, Y. Tamura, S. Takata, T. Mori and N. Ogawa, *Thin Solid Films*, 1994, **246**, 86.

25 F. Leiter, H. Alves, D. Pfisterer, N. G. Romanov, D. M. Hofmanna and B. K. Meyer, *Phys. B*, 2003, **340–342**, 201.

26 P. J. Rostan, J. Mattheis, G. Bilger, U. Rau and J. H. Werner, *Thin Solid Films*, 2005, **480–481**, 67.

27 B. Y. A. Rashid, H. P. Kim and J. Jang, *Org. Electron.*, 2012, **13**, 2379.

28 J. H. Kwak, W. K. Bae, D. G. Lee, L. S. Park, J. H. Lim, M. J. Park, H. D. Cho, H. J. Woo, D. Y. Yoon, K. H. Char, S. H. Lee and C. H. Lee, *Nano Lett.*, 2012, **12**, 2362.

29 M. J. Alam and D. C. Cameron, *J. Vac. Sci. Technol., A*, 2001, **19**, 1642.

30 Y. H. Kim, S. M. Kim, J. W. Kang and C. J. Han, *SID Digest*, 2011, **42**, 1505.

31 Y. S. Kim and W. P. Tai, *Appl. Surf. Sci.*, 2007, **253**, 4911.

32 V. Musat, B. Teixeira, E. Fortunato, R. C. C. Monteiro and P. Vilarinho, *Surf. Coat. Technol.*, 2004, **180–181**, 659.

33 Q. Xu, H. Deng, Y. Li, Q. H. Guo and Y. R. Li, *Mater. Res. Bull.*, 2006, **41**, 354.

34 W. K. Bae, J. H. Kwak, J. W. Park, K. H. Char, C. H. Lee and S. H. Lee, *Adv. Mater.*, 2009, **21**, 1690.

35 Universal Display Corporation, http://www.universaldisplay.com/.

36 A. K. Pandey and J.-M. Nunzi, *Adv. Mater.*, 2007, **19**, 3613.

37 J. P. Lin and J. M. Wu, *Appl. Phys. Lett.*, 2008, **92**, 134103.

38 B. B. Diouf, W. S. Jeon, J. S. Park, J. W. Choi, Y. H. Son, D. C. Lim, Y. J. Doh and J. H. Kwon, *Synth. Met.*, 2011, **161**, 2087.

This journal is © The Royal Society of Chemistry 2013

J. Mater. Chem. C, 2013, **1**, 1567–1573 | **1573**